Walking Ferroelectric Liquid Droplets with Light

Stefano Marni, Giovanni Nava, Raouf Barboza, Tommaso Giovanni Bellini,* and Liana Lucchetti*

The motion of ferroelectric liquid sessile droplets deposited on a ferroelectric lithium niobate substrate can be controlled by a light beam of moderate intensity irradiating the substrate at a distance of several droplet diameters from the droplet itself. The ferroelectric liquid is a nematic liquid crystal, in which almost complete polar ordering of the molecular dipoles generates an internal macroscopic polarization locally collinear to the mean molecular long axis. Upon entering the ferroelectric phase, droplets are either attracted toward the center of the beam or repelled, depending on the side of the lithium niobate exposed to light irradiation. Moreover, moving the beam results in walking the ferroelectric droplet over long distances on the substrate. This behavior is understood as due to the coupling between the polarization of the ferroelectric droplet and the polarization photoinduced in the irradiated region of the lithium niobate substrate. Indeed, the effect is not observed in the conventional nematic phase, suggesting the crucial role of the ferroelectric liquid crystal polarization.

1. Introduction

The recent discovery of the ferroelectric nematic phase, N_F,[1] opened a new chapter not only for the liquid crystal (LC) community, but also for the whole condensed-matter physics. Besides adding a new, very peculiar, member to the group of ferroelectric materials, the new phase offers a broad range of physical effects to explore, ranging from the behavior of topological defects to surface anchoring,[2] response to low-frequency electric fields[3] and light, interplay of bound and free electric charges, viscoelastic properties, field-controlled hydrodynamics,[3–5] field-order coupling in both the N_F and

S. Marni, R. Barboza, L. Lucchetti
Dipartimento SIMAU
Università Politecnica delle Marche
via Brecce Bianche, Ancona 60131, Italy
E-mail: l.lucchetti@univpm.it
G. Nava, T. G. Bellini
Medical Biotechnology and Translational Medicine Dept.
University of Milano
Segrate 20054, Italy
E-mail: tommaso.bellini@unimi.it

The ORCID identification number(s) for the author(s) of this article can be found under https://doi.org/10.1002/adma.202212067.

the pretransitional regions, behavior in confined geometry,[6] just to cite a few examples. In this scenario, we recently performed experiments devoted to characterize the behavior of sessile N_F droplets on ferroelectric solid substrates[4] and found that the combination of fluidity and polarity gives rise to an electromechanical instability induced by the coupling of the LC polarization with that pyroelectrically induced in the solid substrate.

In this work, we instead analyze the effects of the photovoltaic charging of lithium niobate (LN) ferroelectric solid substrates on N_F sessile droplets, at constant temperature. The advantages of manipulating sessile droplets by light are related to the possibility of focusing the beam to small regions of the substrates, thus limiting the extent of the charged regions and controlling its distance and position with respect to the droplets, and of quickly reconfiguring it in different illumination geometries. Results show that, under proper experimental conditions, light irradiation gives rise to an instability very similar to the one observed in ref. [4]. Moreover, focused beams impinging on the LN substrate at a certain distance from the sessile N_F droplets allow us to optically control their motion. Droplets are attracted toward the center of the illuminated area or repelled away from it depending on which side of the substrate is exposed to light irradiation and can be walked by the light beam over long distances. Our results contribute an additional piece to the collection of intriguing features characterizing the ferroelectric nematic phase, and may have potential for future applications.

Worthy of note, light-induced dynamics of liquid crystal droplets on the surface of iron-doped LN crystals has recently been studied for both conventional nematics and compounds exhibiting the ferroelectric nematic phase.[5] A wide range of interesting dynamic phenomena have been described; some of them probably related to the electromechanical instability of ferroelectric liquid droplets. However, no optical control of droplets motion was reported.

2. Results

Our first experiment has been devoted to compare the effect of photoinduced charging of LN substrates on RM734 sessile droplets, with the one of pyroelectric charging that we recently reported in ref. [4]. To this purpose, LN was irradiated in correspondence of the droplet position with an unfocused Gaussian
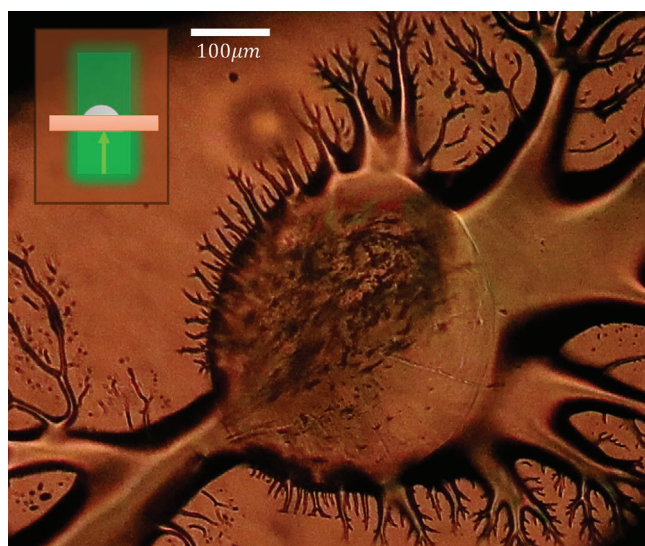
Figure 1. RM734 sessile droplet on LN substrate exposed to light illumination. The beam diameter is slightly larger than that of the droplet, as shown in the cartoon on the left-hand side. Shape instability with the emission of interfacial fluid jets that bifurcate and branch is clearly visible (figure extracted from Video S1 in the Supporting Information). $I = 20$ W cm^{-2}. Droplet diameter = 350 µm.

beam having a diameter slightly larger than that of the droplet itself. As shown in **Figure 1**, such a configuration produces an electromechanical instability consisting in the sudden emission of interfacial fluid jets, as observed in ref. [4], indicating that the coupling between the droplet polarization and the one photoinduced in LN has the same features as the coupling with the pyroelectrical LN polarization. In analogy to the interpretation proposed there, we understand this phenomenon as due to the fringing field generated by the photovoltaic charging of LN

substrates, which is thus able to affect the N_F droplets behavior. This result opens the way to the possible optical control of ferroelectric LC droplets on LN substrates. Indeed, light is easily controllable; the size and the position of the irradiated region can be varied almost at will and the intensity of the light beam can be tuned in a very short time.

The effect reported in Figure 1 is independent on the side of the LN substrate contacting the droplet. This is in agreement with the observations in ref. [4], where the sign of the charges of the LN surface that contacts the LC droplet was irrelevant.

The same fringing field generated by photovoltaic charging leads to new effects when the light beam is focused at a distance from the droplets. In this case, the droplet retains approximately the same shape but is put in motion by a force generated by light irradiation. Remarkably, the direction of such a force can be either attractive, with droplets that move toward the center of the illuminated region, or repulsive, leading to a droplet motion away from the light spot. The sign of the force depends on the irradiated side of the LN substrate. This is illustrated in **Figure 2**, which shows two series of frames extracted from Video S2 (Supporting Information) (Figure 2b–d) and Video S3 (Supporting Information) (Figure 2b′–d′). As visible, a N_F droplet moves toward the illuminated area or away from it, depending on the direction of the LN bulk polarization with respect to the direction of the incoming light (as in the cartoons on the left-hand side of the figure), which we will refer to as "UP" and "DOWN" in the rest of the paper.

By continuously varying the position of the beam by means of galvanometric mirrors, it is possible to drag the N_F droplet over long distances, as shown in **Figure 3** in the case of droplet attraction (frames extracted by Video S4 in the Supporting Information). Droplet dragging is also observed in case of repulsion, although with a less controlled trajectory.

The curves describing droplet motion versus time are reported in **Figure 4** in case of both the UP (a) and the
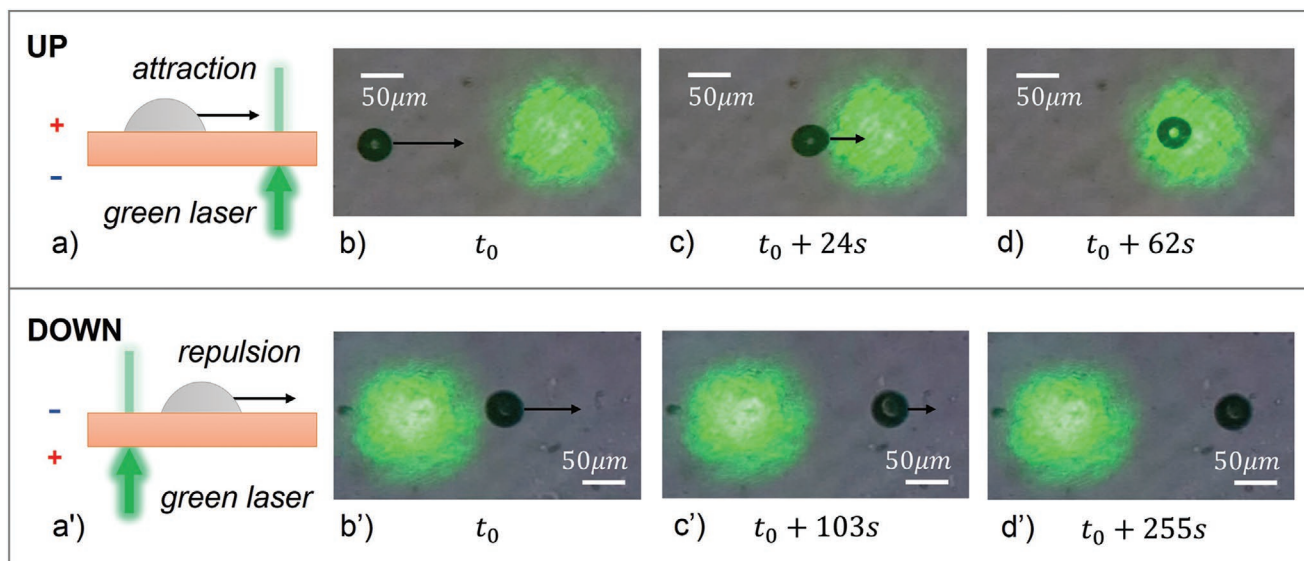

Figure 2. a,a′) Sketches of the experimental arrangements in case of droplet attraction (a) and repulsion (a′). b,c,d) Video frames taken at different instants showing an RM734 N_F droplet moving toward the center of the illuminated area. b′,c′,d′) Video frames taken at different instants showing an RM734 N_F droplet moving away from the center of the illuminated area. $I = 5 \times 10^2$ W cm^{-2}.
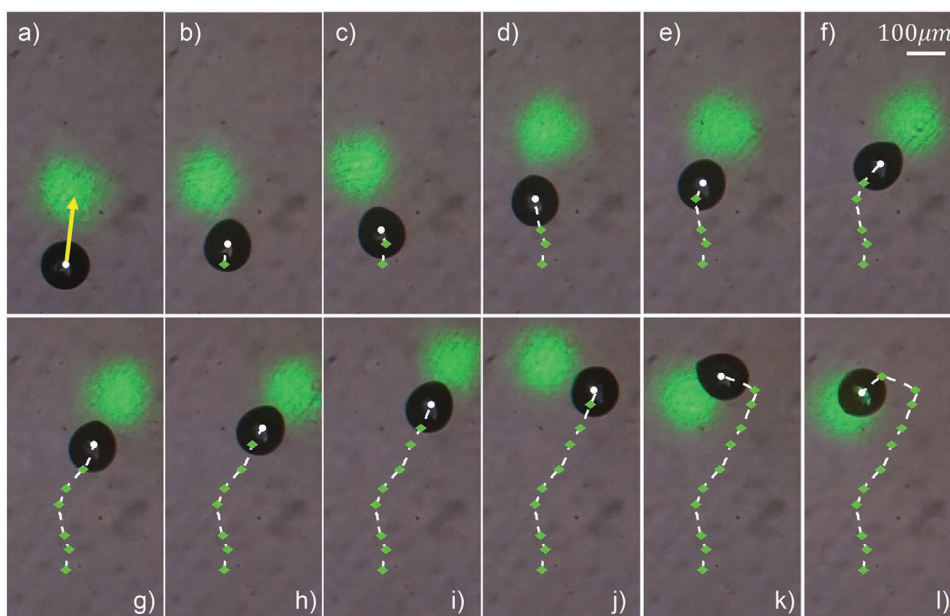
Figure 3. a–l) Video frames at different instants showing the motion of an RM734 N_F droplet following a Gaussian light spot along a wavy path. The green diamonds indicate the different positions of the droplets through the video, and the dashed line represents the droplet trajectory. $I = 3 \times 10^2$ W cm^{-2}.

DOWN (b) cases. The different curves in each figure refer to different values of the light intensity. Different initial distances between droplet and light spot center have also been chosen to highlight the role of both these parameters.

To avoid superpositions and improve the clarity of the two graphs, some of the curves have been translated in time. Remarkably, the curve corresponding to the lowest beam intensity in Figure 4b (red curve in panel DOWN), shows
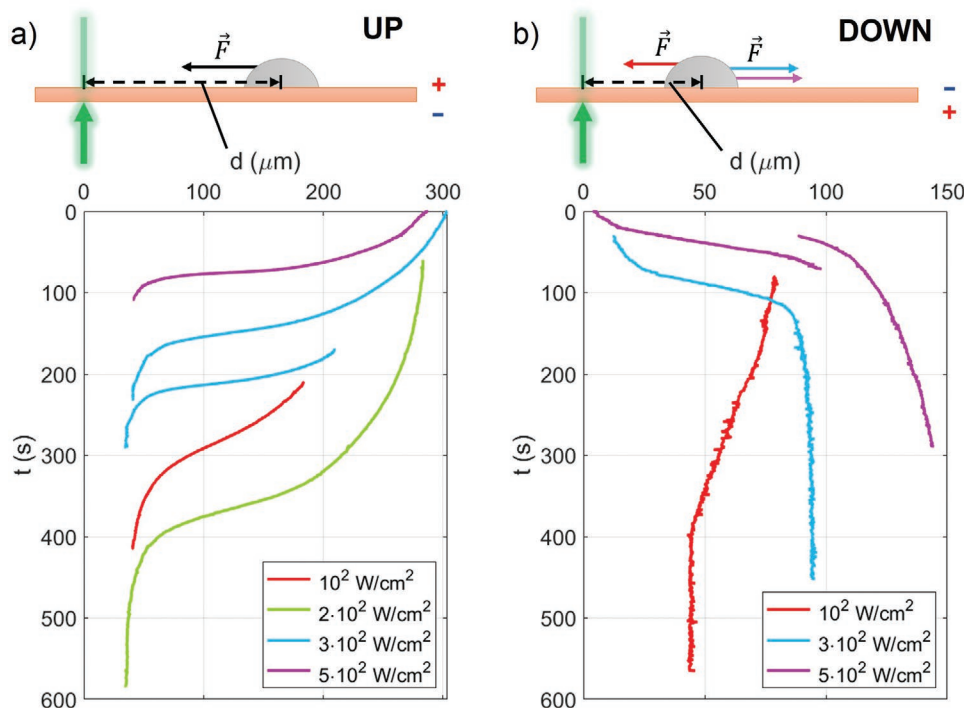

Figure 4. Droplet distance from the center of the illuminated area ($d = 0$) as a function of time, for the UP (a) and DOWN (b) cases. The time $t = 0$ s corresponds to the beginning of LN illumination, however, to improve the clarity of the figure; some of the curves have been shifted in time so to start at $t > 0$ s. Different colors indicate different values of the light intensity as reported in the legend; different starting distances have also been chosen. The two cartoons on top help defining the parameters and understanding the experimental arrangement in the two conditions.
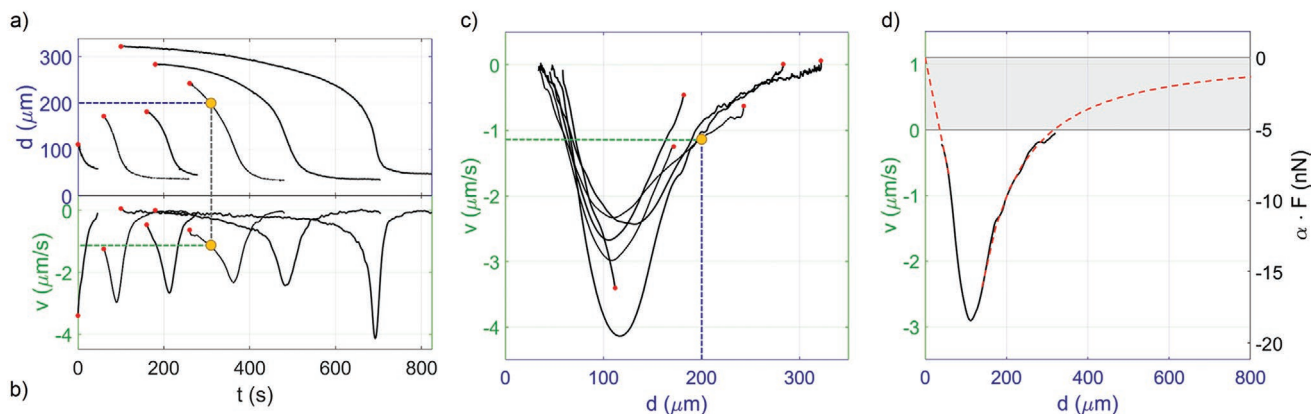
Figure 5. Steps leading to determine the dielectrophoretic force profile as a function of the distance between N_F droplet and light spot center. a) Droplet distance from the light spot center for fixed light intensity and different starting positions and b) the corresponding droplet velocity as a function of time. Red dots indicate different starting positions while yellow dots identify the values of d and v corresponding to the same time instant. c) Droplet velocity as a function of the distance from the light spot center, obtained combining (a) and (b). Red dots indicate different starting positions while the yellow dot has the coordinates (d,v). d) Average velocity (left) and dielectrophoretic force (right). The red dashed line on the left is a linear extrapolation of the velocity at $d = 0$. The one on the right is a best fit of the force for $d > 140$ μm. The parameter α $(0 < \alpha < 1)$ indicates that the real values of F are higher than those reported in the graph (see the text). The gray area corresponds to values of F, not enough high to overcome friction and generate droplet motion. $I = 2 \times 10^2$ W cm^{-2}.

droplet motion toward the light spot, contrary to what happens at higher intensity.

A close inspection of Figure 4 reveals that N_F droplets attracted toward the illuminated area stop at the edge of a region corresponding to the beam waist (Figure 4a); N_F droplets repelled by the illuminated area also stop at a certain distance from their center that increases with increasing light intensity. This behavior suggests the presence of a pinning force opposing to the one due to the interaction with the light beam.

From these and similar curves, it is possible to extract the time dependence of the droplet velocity v for each used value of the light intensity I. As an example, **Figure 5**b shows v versus t in the case of droplet attraction and $I = 2 \times 10^2$ W cm^{-2}, for different initial distances from the center of the illuminated area, as extracted from the corresponding d versus t curves reported in Figure 5a. Again, for the sake of clarity, some of the curves are shifted in time. Red dots indicate the initial conditions in terms of initial distance from the light spot center and initial droplet velocity. The three dashed lines identify the values of d and v corresponding to the same value of t. Combining the v vs t curve with the corresponding d vs t, one obtains the velocity as a function of the distance from the center of the illuminated area. This is shown in Figure 5c, where the different curves refer to different initial droplet positions with respect to the center of the light spot. Interestingly, despite a relevant irregularity, the velocity keeps similar values at fixed positions, that is, its value is independent on the initial position of the droplet. This indicates that droplets' inertia can be neglected in describing the droplet motion, demonstrating that the friction force contains a term dependent on v. The average velocity $\langle v \rangle$ is reported in Figure 5d.

To better understand droplet motion, a friction characterization is necessary. To this aim, we performed measurements of droplet motion along a tilted substrate in the absence of light, using a nematic LC of lower viscosity (see the Supporting

Information) to facilitate the experiment. Such measurements showed that friction is indeed composed of two parts: one constant term due to pinning acting as a kinetic friction, and one viscous term proportional to the droplet velocity and due to the internal fluid motion. The equation of motion, neglecting inertia, is thus $F = f_{pinning} + \mu_v v$, where F is the force, attractive or repulsive, due to the action of light and μ_v is the viscous friction coefficient.

We understand the coupling of the droplet to light as mediated by the fringing field generated by the charge accumulation due to the photovoltaic properties of LN crystals. The simplest form of such coupling is through dielectrophoresis.[7] As a consequence, we expect F to become negligible in the center of the illuminated area $(d = 0)$, where electric field gradients vanish because of symmetry. Therefore, by extrapolating the value of $\langle v \rangle$ for $d = 0$ (1.1 μm s^{-1} in Figure 5d, the red dashed line on the left of the curve), we obtained a relationship between the two friction terms; the pinning force has the value that the viscous friction would have for $\langle v \rangle = v$ $(d = 0)$. In this way, the force F can be written as $F = \mu_v (\langle v \rangle + \langle v$ $(d = 0) \rangle)$, i.e., F is proportional to v through the viscous friction coefficient and thus its dependence on the distance d resembles that of $\langle v \rangle$, as shown in the right part of Figure 5d. The dashed red line on the right is the power law $(F = 18d^{(-1.5)}$, with d in μm that better approximates the force in the range of (140–320) μm. An estimation of the lower bound of the viscous friction coefficient μ_v has been obtained by performing measurements on tilted LN substrate illuminated so to induce N_F droplet motion toward the top or toward the bottom, as described in the Supporting Information. Since, within the experimental errors, the velocity is the same in the two situations, we could estimate that μ_v is larger than the ratio between twice the component of the gravitational force along the substrate and the uncertainty in the velocity value (see the Supporting Information). Since we used the lower bound for μ_v, the values of the
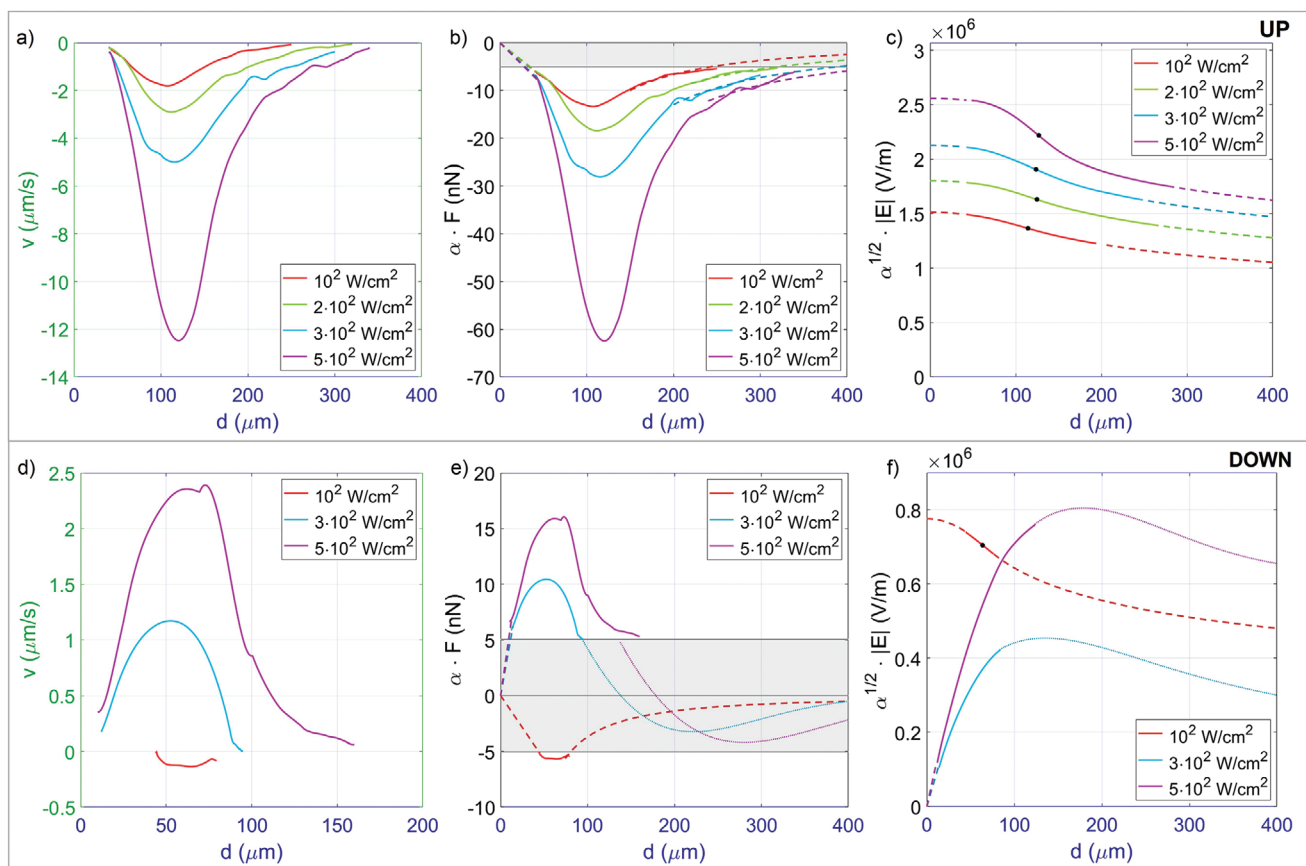
Figure 6. a–f) Average droplet velocity, dielectrophoretic force, and electric field as a function of the droplet distance d from the light spot center, for the UP (a–c) and DOWN (d–f) cases. Different colors indicate different values of the light intensity. The gray areas in (b) and (e) are regions of no droplet motion, i.e., regions where the dielectrophoretic force is too weak to overcome friction. In the same panels, dashed lines are power laws that approximate the trend of the forces for values of d outside the actual tracking, while dotted lines are virtual extensions of the real profiles to regions where forces could not be derived from experimental data, due to the absence of motion. The dashed and dotted lines in (c) and (f) represent regions of field values derived from these parts of the dielectrophoretic forces that do not come from experimental data. The black spots in (c) and (f) mark the inflection points of the curves thus identifying the fields range.

dielectrophoretic force are higher than those in Figure 5d by a certain amount. We quantified this unknown amount with the number α, in the range $0 < \alpha < 1$. The gray area indicates the region within which the force exerted on the droplet is not high enough to overcome friction and generate droplet motion.

The average velocities as a function of the droplet distance d from the center of the illuminated area, for all the used values of the light intensity, are reported in **Figure 6** for both the UP (a) and DOWN (d) cases. Note that the average droplet velocities are negative in panel (a) indicating droplet motion toward the light spot, and positive in panel (d), indicating motion away from the light spot, for all the values of I but the lowest. In this case, $\langle v \rangle$ is negative both in panels (a) and (d). As for the values, at a fixed light intensity, $\langle v \rangle$ is sensitively higher in case of attractive droplet motion and so is the covered distance. This is also translated in the force profile, which are shown in Figure 6b,e. Both the values and the range are larger in panel (b) than in panel (e), suggesting different values and profiles of the fringing fields responsible for the dielectrophoretic force. In extrapolating the pink and blue curves in Figure 6e for

large d, we assumed that F would become negative before vanishing at large distances. This is because the electric field has to vanish at large d and thus a range in which dE/dd is negative is required. At the lowest intensity, the force becomes positive (red curve) and is analogous to F in Figure 6b.

To evaluate the electric field profile, we considered the explicit form of the dielectrophoretic force, which is available for the simpler case of spherical shape droplets.[7] In this case, F depends on the gradient of the electric field squared as

$$F = 2\pi R^3 \varepsilon_m \operatorname{Re}\left[\frac{\varepsilon_p - \varepsilon_m}{\varepsilon_p + 2\varepsilon_m}\right] \nabla E^2 \qquad (1)$$

where R is the radius of a sphere of complex dielectric permittivity $\varepsilon_p = \varepsilon'_p + i\frac{\sigma_p}{\omega\varepsilon_0}$, dispersed in a medium of complex dielectric permittivity $\varepsilon_m = \varepsilon'_m + i\frac{\sigma_m}{\omega\varepsilon_0}$. σ_p and σ_m are the conductivities of the particle and of the medium, respectively.

When either particle or medium is conductive, at low frequency the imaginary part of the permittivity prevails, and the force becomes[8]

**ADVANCED
SCIENCE NEWS**

www.advancedsciencenews.com

**ADVANCED
MATERIALS**

www.advmat.de

$$F = 2\pi R^3 \varepsilon_m \left[\frac{\sigma_p - \sigma_m}{\sigma_p + 2\sigma_m} \right] \nabla E^2 \approx 2\pi R^3 \nabla E^2 \qquad (2)$$

Although in a strict sense RM734 is an insulator, the availability of readily displaceable polarization charges makes droplets in the N_F phase behave as conductive droplets since their displaced polarization charges cancel any field internal to the material.[4,6] This is the reason why ferroelectric nematics exhibit an effectively large dielectric coefficient. For this reason, the ratio in square brackets in Equation (2) becomes equal to one and, being $\varepsilon_m = 1$, the gradient of the field squared can be expressed as the ratio between the force and a term depending on the droplet's volume.

Equation (2) is a rough approximation since i) the sessile droplet is more similar to a hemisphere than to a sphere and ii) the droplet is on the top of LN whose dielectric properties are relevant and can locally compensate the surface polarization charges displaced in RM734. We thus argue that Equation (2) overestimates the dielectric force acting in our observations.

Interestingly, the reported optical control of LC droplets has been observed only in the ferroelectric phase. No light-induced droplet movement has been observed in the RM734 N phase or using conventional nematic liquid crystals, such as pentylcyano-biphenyl (5CB). We understand this behavior as a clear indication that the dielectrophoretic interaction is different in the N and N_F phases. Results suggest that the dielectrophoretic interaction is stronger when droplets are in the ferroelectric phase, while it is not strong enough to overcome the pinning force in the nematic phase. This is in agreement with the fact that the limiting condition of the Clausius–Mossotti ratio in the right-hand side of Equation (2) corresponds to its largest possible value. The situation is very different in the N phase, since in this case the permittivity of LC and LN substrates both has values in the range of 50–100, leading to a much lower Clausius–Mossotti ratio.

The electric field responsible for the dielectrophoretic force can be obtained by integrating the force itself and is reported in Figure 6c (UP) and Figure 6f (DOWN), as a function of the distance from the center of the light beam for different values of I. A comparison of the two sets of curves shows differences in the field profiles, maximum values, and range. Specifically, both the range and the maximum values are higher in Figure 6c, which correspond to droplet motion toward the center of the light spots. Moreover, maxima are located close to the center of the light spot or at a certain distance that increases with light intensity, depending on the direction of the droplets' motion. The red curve in Figure 6f, which corresponds to droplet attraction, is similar in shape to that in Figure 6c but with smaller maximum value and range.

The electric field responsible for the dielectrophoretic forces acting on the N_F droplets is the fringing field produced by the LN charging due to light irradiation. Although this effect could easily be attributed to the well-known photovoltaic response of LN, the contrasting behavior observed upon inverting the LN crystal, points to a more complex causal chain. A further clue of such complexity is the inconsistency between the expected independence of the LN photovoltaic field on light intensity for values of I up to about 10^3 W cm^{-2},[9] and the observation showing a field that clearly depends on I.

It should also be noted that the range of the attractive force in the UP case is significantly larger than the laser beam waist (100 vs 35 μm). Among the effects known to take place in LN, the pyroelectric effect is the one most compatible with this observation; in the UP case, the range of the force reflects that of local temperature rise due to absorption. Light-induced heating of the LN substrate can be evaluated through the following expression: $\Delta T = \left(\frac{1}{w^2} + \frac{\pi^2}{d^2} \right)^{-1} \frac{\alpha}{K} I$, being w the beam waist, d the LN thickness, α the absorption coefficient, and K the thermal conductivity. Using for K the value 10^{-2} cal s^{-1} cm^{-1} °C^{-3} valid for undoped crystals (which is expected to be lower than the one of iron-doped LN) and for α the value 5 cm^{-1} measured for green light in similar crystals,[10] the maximum temperature rise at steady state is of the order of a few degrees Celsius. This can give rise to a pyroelectric charging yielding an electric field of the same order of the photovoltaic field.[10] The repulsive force in the DOWN case appears instead to have a shorter range, more compatible with the illuminated area, suggesting that photovoltaic and pyroelectric effects may sum up differently on the two sides. However, such a difference necessarily requires the symmetry between positive and negative charges on the two LN sides to be broken. Any process that would equally modify positive and negative charges, such as a local modulation of the ferroelectric bulk polarization of LN, could not explain our observations. Indeed, the absorbance of the laser green light by the iron-doped LN provides such a symmetry breaking, since the directly irradiated LN side is the location of largest density of iron electron excitation. We reasonably expect such freed electrons to adopt a different spatial distribution when close to the positive versus negative LN surface.

Noteworthy, asymmetry of the two surfaces of z-cut LN crystals has already been observed in the literature,[10–12] both in relation to the efficiency of the surfaces in generating electrostatic fields,[11,12] that have been reported to be different for $-z$ and $+z$ surfaces, and in relation to the asymmetric behavior of liquid crystals confined in LN microchannels under light illumination.[10] In this latter case, the combination of photovoltaic and pyroelectric fields was invoked to account for a liquid crystal response dependent on the irradiated surface in an optofluidic chip based on z-cut LN crystals.

3. Conclusion

We have demonstrated the all-optical control of sessile ferroelectric liquid droplets deposited on lithium niobate substrates. Droplets are attracted or repelled by the center of the illuminated region depending on the irradiated side of the LN crystal with a range of interaction that is sub millimetric in our conditions, but that may increase by using different surface coatings. Droplets can also be walked by the light beam over long distances. The reported droplet actuation is observed only in the N_F phase, which highlights the crucial role played by the RM734 ferroelectric polarization.

Based on our results, we expect that by reconfiguring the experimental apparatus and structuring light with a spatial light modulator, all the basic droplet handling operations required in

a common microfluidic device can be obtained. This opportunity may pave the way to novel technological applications triggered by the peculiar properties of ferroelectric nematics.

To give a few potential examples, the possibility of optically controlling the motion of ferroelectric liquid droplets over ferroelectric solid substrates might have high impact in the field of micro and optofluidics, where the manipulation of complex fluids is still widely unexplored. As we have shown, the behavior of ferroelectric and nematic droplets on the structured polarization of the substrate is different, which may pave the way to the use of RM734 droplets as switchable sensors of external electric fields. In addition, the ability to optically control body forces on ferroelectric nematic droplets might provide the basis for electro-hydromechanical applications like soft robotics.

We believe that the results reported here contribute an additional piece to the collection of intriguing features characterizing the ferroelectric nematic phase.

4. Experimental Section

The ferroelectric liquid crystal used in this work was 4-[(4-nitrophenoxy)carbonyl]phenyl2,4-dimethoxybenzoate (RM734). It was synthesized as described in ref. [1], and its structure and phase diagram were already reported.[1,2,4] In this compound, the ferroelectric nematic phase appears through a second-order phase transition when cooling from the conventional higher temperature nematic (N) phase and exists in the range $133\ °C < T < 80\ °C$.[2,4] The spontaneous polarization **P** of RM734 is either parallel or antiparallel to the molecular director **n**, defining the average orientation of the molecular axis, and exceeds 6 μC cm^{-2} at the lowest T in the N$_F$ phase.[1]

The LN ferroelectric substrates were 900 μm thick z-cut crystals. Experiments were performed on iron-doped substrates containing 0.1% mol. of iron with a reduction factor, $R = 0.02$. The bulk spontaneous polarization P_{LN} of LN crystals along the [0001] z-axis is of the order of 70 μC cm^{-2} and does not depend significantly on T in the explored range since its Curie temperature is much higher ($\approx$1140 °C). The huge bulk polarization of LN does not however translate in a huge surface charge density because of very efficient compensation mechanisms at the z-cut surfaces, lowering the equilibrium surface charge to only about 10^{-2} μC cm^{-2}.[13] When the crystal was exposed to light with wavelength in the iron absorption spectrum, the surface charge of LN significantly increased because of the photovoltaic effect,[9] consisting in the appearance of a photoinduced current according to the scheme $Fe^{2+} + h\nu \rightarrow Fe^{3+} + e^-$. The subsequent charge distribution that takes place inside the crystal gives rise to an internal electric field with saturation values up to 10^7 V m^{-1}, depending on the dopant concentration and on R.[9,14] In the specific case of the LN crystals used here, a photovoltaic field $E_{PV} = (10.1 \pm 0.8)$ V μm^{-1} was measured.[14] Before droplet deposition, LN crystals were coated by a layer of fluorolink. This polymer was selected because it features lower surface coupling of RM734 molecules, than Teflon, silane, and hydroxylated glass.[2] It thus provides the best conditions for observing RM734 droplets motion. Fluorolink coating was obtained as described in ref. [2]. The average contact angles of RM734 droplets on coated LN were 73° in the isotropic phase and 70° in the N phase, and decreased to 55° in the N$_F$ phase, thus showing larger values than in ref. [4], but the same trend.

The RM734 droplets used in optical motion control experiments had an average diameter of 45 μm, as measured with a calibration slide and were obtained starting from bigger droplets as described in the Supporting Information. They were deposited on fluorolink-coated LN substrates that were previously slowly heated up to $T = 200\ °C$, corresponding to the RM734 isotropic phase. Successively, T was decreased down to 110 °C, which is in the ferroelectric range. This value of temperature was selected in the range of 120–100 °C, where droplet

motion is predictable and highly reproducible. Between 133 and 120 °C, droplet velocity exhibited strong fluctuations and for $T < 100\ °C$ the motion became very slow because of the increase of viscosity close to the crystalline phase. Noteworthy, the cooling rate was kept slow enough to avoid the droplets electromechanical instability observed in ref. [4] that was triggered by the pyroelectric charging of LN surfaces and required a proper cooling speed.

The light used to induce the photovoltaic effect in LN crystals was a Gaussian beam from a frequency doubled neodimium-doped yttrium aluminium garnet (Nd:YAG) laser ($\lambda = 532$ nm), with power P in the range of (5–25) mW, focused to a waist $w = 35$ μm, which corresponds to an intensity ranging from $I = 10^2$ W cm^{-2} to $I = 5 \times 10^2$ W cm^{-2}. LN substrates were irradiated from below at different distances to the RM734 droplets, holding the temperature fixed at $T = 110\ °C$. Polarized optical microscopy (POM) observations during light irradiation were carried out and videos of the droplets behavior were recorded with a rate of 25 fps.

Supporting Information

Supporting Information is available from the Wiley Online Library or from the author.

Conflict of Interest

The authors declare no conflict of interest.

Data Availability Statement

The data that support the findings of this study are available from the corresponding author upon reasonable request.

[1] X. Chen, E. Korblova, D. Dong, X. Wei, R. Shao, L. Radzihovsky, M. A. Glaser, J. E. Maclennan, D. Bedrov, D. M. Walba, A. Clark, *Proc. Natl. Acad. Sci. USA* **2020**, *117*, 14021.

[2] F. Caimi, G. Nava, R. Barboza, N. A. Clark, E. Korblova, D. M. Walba, T. Bellini, L. Lucchetti, *Soft Matter* **2021**, *17*, 8130.

[3] M. T. Mathè, A. Buka, A. Jakly, P. Solomon, *Phys. Rev. E* **2022**, *105*, L052701.

[4] R. Barboza, S. Marni, F. Ciciulla, F. A. Mir, G. Nava, F. Caimi, A. Zaltron, N. Clark, T. Bellini, L. Lucchetti, *Proc. Natl. Acad. Sci. USA* **2022**, *119*, e2207858119.

[5] A. Sterle, L. Cmok, N. Sebastián, A. Mertelj, Y. Kong, X. Zhang, I. Drevenšek-Olenik, *Opt. Mater. Express* **2023**, *13*, 282.

[6] F. Caimi, G. Nava, S. Fuschetto, L. Lucchetti, P. Paiè, R. Osellame, X. Chen, N. A. Clark, M. Glaser, T. Bellini, arXiv:2210.00886 **2022**.

[7] A. Zaltron, D. Ferraro, A. Meggiolaro, S. Cremaschini, M. Carneri, E. Chiarello, P. Sartori, M. Pierno, C. Sada, G. Mistura, *Adv. Mater. Interfaces* **2022**, *9*, 2200345.

[8] D. A. Saville, T. Bellini, V. Degiorgio, F. Mantegazza, *J. Chem. Phys.* **2000**, *113*, 6974.

[9] T. Volk, M. Wöhlecke, *Lithium Niobate: Defects, Photorefraction and Ferroelectric Switching*, Vol. *115*, Springer Science & Business Media, Berlin, Germany **2008**.

[10] S. Bonfadini, F. Ciciulla, L. Criante, A. Zaltron, F. Simoni, V. Reshetnyak, L. Lucchetti, *Sci. Rep.* **2019**, *9*, 1062.

[11] Z. Gao, Y. Mi, M. Wang, X. Liu, X. Zhang, K. Gao, L. Shi, E. R. Mugisha, H. Chen, W. Yan, *Opt. Exp.* **2021**, *29*, 3808.

[12] F. Li, X. Zhang, K. Gao, L. Shi, Z. Zan, Z. Gao, C. Liang, E. R. Mugisha, H. Chen, W. Yan, *Opt. Exp.* **2019**, *27*, 25767.

[13] S. Sanna, W. G. Schmidt, *J. Phys.: Condens. Matter* **2017**, *29*, 413001.

[14] L. Lucchetti, K. Kushnir, V. Reshetnyak, F. Ciciulla, A. Zaltron, C. Sada, F. Simoni, *Opt. Mater.* **2017**, *73*, 64.